Journal of Materials Chemistry A

ROYAL SOCIETY OF CHEMISTRY

PAPER

View Article Online
View Journal | View Issue

Cite this: J. Mater. Chem. A, 2020, 8, 9677

A one-step rapid synthesis of TS-1 zeolites with highly catalytically active mononuclear TiO_6 species†

Wenjing Xu,‡[a] Tianjun Zhang, ‡[ac] Risheng Bai, [a] Peng Zhang[c] and Jihong Yu *[ab]

The modulation and determination of the coordination environments of Ti active sites in titanosilicate zeolites are key challenges in the rational design of high-performance heterogeneous catalysts. Up to now, the highly catalytic active Ti species, while not yet unambiguously determined, is mainly constructed by the complex post-treatment method, in which it is difficult to precisely control the distribution of the created Ti species. Herein, we showcase a facile strategy for the one-step rapid synthesis of TS-1 (**MFI** framework type) zeolites with highly catalytically active Ti species *via* active seed-assisted microwave irradiation. The coordination environment and local structure of the Ti species in TS-1 zeolites were investigated *via* UV-vis, UV-Raman, and X-ray absorption spectroscopies. Significantly, according to the elaborate characterizations based on the extended X-ray absorption fine structure (EXAFS), these highly catalytically active Ti species were clearly identified as novel mononuclear TiO_6 species. Experimental studies revealed that the active seeds can provide plenty of high-coordinated Ti precursors, which play a critical role in creating mononuclear TiO_6 in the zeolite framework coupled with microwave irradiation. Moreover, such mononuclear TiO_6 species remain stable upon calcination. The obtained catalyst affords a high turnover number value (272) in the 1-hexene epoxidation reaction, which is almost 70% higher than that of the conventional TS-1 zeolite (161). This study may open new perspectives for the designed synthesis and applications of titanosilicate zeolite catalysts in various important selective oxidation reactions.

Received 18th December 2019
Accepted 20th April 2020

DOI: 10.1039/c9ta13851j

rsc.li/materials-a

Introduction

Zeolites are a unique class of crystalline porous materials with well-defined pores and channels at the molecular level, and have found a variety of applications in the chemical industry.[1–3] As one of the most important members of the zeolite family, Ti-containing zeolites have been studied extensively with regards to a series of selective oxidation reactions, such as alkene epoxidation,[4–8] ketone ammoximation,[9] and phenol oxidation.[10]

To enhance the catalytic performance of such catalysts, great efforts have been made in tailoring the crystal sizes or building the hierarchical structures of Ti-containing zeolites, such as TS-1 (**MFI**), Ti-**MWW**, Ti-**MOR**, and Ti-beta (***BEA**).[11–16] However, as a key factor in the catalytic reactions, the exact nature of different Ti active sites remains unclearly unraveled. The density functional theory (DFT) calculations showed that a new kind of Ti sites, which are located at adjacent Si vacancies in the TS-1 lattice, were more reactive than fully coordinated Ti sites in propylene epoxidation.[17] This finding pointed out a promising way to improve the catalytic performance of Ti-containing zeolites, namely, tuning the chemical environment of the Ti active centers. Typically, both an increase in the Lewis acid strength of the titanium species and the adjustment of the Ti coordination states can lead to a significant enhancement in catalytic behaviors.[18–22]

To date, several strategies have been proposed to modify the Ti active centers in Ti-containing zeolites.[23–27] For instance, Fang *et al.* reported a strategy to increase the electropositivity of the Ti active sites in the Ti-**MWW** zeolite by implanting the F species on the neighboring framework Si, and thus the catalytic property of such Ti species got enhanced.[23] However, the simultaneously formed harmful F species, which lowered the catalytic property of the Ti active sites, must be eliminated afterward. To overcome the complex synthetic procedure, in some other cases, the Ti active sites were directly modified *via*

[a]State Key Laboratory of Inorganic Synthesis and Preparative Chemistry, College of Chemistry, Jilin University, Changchun 130012, P. R. China. E-mail: jihong@jlu.edu.cn

[b]International Center of Future Science, Jilin University, Changchun 130012, P. R. China

[c]Department of Chemistry, Dalhousie University, Halifax, Nova Scotia B3H 4R2, Canada

† Electronic supplementary information (ESI) available: Experimental and characterization processes, SEM images, textural properties, UV-vis spectra, UV-Raman spectra, XPS spectra, FT-IR spectra and the EXAFS fitting results of different TS-1 zeolites and the results of 1-hexene epoxidation reactions over TS-1-CM and TS-1-AM. See DOI: 10.1039/c9ta13851j

‡ These authors contributed equally.

the post-treatment approach. For instance, the pentahedrally and octahedrally coordinated Ti species can be obtained by the hydrothermal treatment of the conventional tetra-coordinated Ti-containing zeolites with different organic amines.[24–26] Meanwhile, with the development of the modern characterization techniques, the local structures of different Ti active sites have been thoroughly investigated.[28–32] Notably, the unique mononuclear TiO_6 in TS-1 established based on UV-Raman and DFT calculations was proposed to be responsible for its excellent catalytic activity in alkene epoxidation.[18,25,26] Therefore, a facile construction as well as elaborate identification of mononuclear TiO_6 has attracted considerable attention in exploring the high-performance Ti-containing zeolite catalysts.

Compared with the conventional hydrothermal synthesis of zeolites, the microwave synthesis method has proven to be a more efficient way to prepare titanosilicate zeolites since the heat-up time can be rapidly and uniformly induced by the microwave irradiation.[33] Moreover, the seed-assisted method has demonstrated its significant impact on the distribution of the Ti species. For instance, the surface of the Ti-enriched TS-1 zeolite can be obtained *via* the seed-assisted intermediate crystallization strategy.[34] In this study, we developed a one-step method to rapidly synthesize TS-1 zeolites with highly catalytically active mononuclear TiO_6 species. By introducing active seeds, which can provide plenty of highly coordinated Ti precursors with the assistance of microwave irradiation, highly crystalline TS-1 zeolites containing mononuclear TiO_6 can be prepared within 1 hour. Significantly, based on X-ray absorption spectroscopy (XAS), we clearly identified the mononuclear state of the TiO_6 species in TS-1 zeolites. The effects of synthesis conditions on the chemical environments of the Ti species as well as catalytic activities of the resultant catalysts were systematically investigated. The obtained results demonstrated that the greatly enhanced catalytic performance of TS-1 zeolites was highly associated with the formation of mononuclear TiO_6. This discovery paves the way for design, synthesis, and catalytic applications of titanosilicate zeolites with active Ti sites.

Experimental

Preparation of conventional TS-1 (TS-1-C), active seeds and calcined seeds

TS-1-C zeolite was synthesized from the starting gel with the molar composition of SiO_2 : $0.0167TiO_2$: 0.4TPAOH : $1.5CH_3CH_2OH$: $23.5H_2O$ under hydrothermal conditions at 170 °C. Typically, tetrapropylammonium hydroxide (TPAOH) and deionized water were mixed completely, and then tetraethylorthosilicate (TEOS) was added dropwise to a mixture of H_2O and TPAOH under vigorous stirring, giving rise to a clear solution. Then, tetrabutylorthotitanate (TBOT) and ethanol were added dropwise to this solution. After the complete hydrolysis of TEOS and TBOT, the resulting solution was transferred into a Teflon-lined stainless steel autoclave and then crystallized in an oven at 170 °C for 1.5 h to 4 d under static condition. The obtained colloidal product was used as active seeds. After separation by centrifuging and drying at 80 °C in an oven overnight, calcination was carried out at 550 °C for 6 h. The calcined product was used as calcined seeds.

Preparation of TS-1-AM and TS-1-CM

TS-1 zeolites were synthesized from the starting gels with the molar compositions of SiO_2 : $(0.0667–0.0167)TiO_2$: 0.4TPAOH : $1.5CH_3CH_2OH$: $23.5H_2O$ under hydrothermal conditions at 170 °C. Typically, TPAOH (25 wt%) and deionized water were mixed completely, and then TEOS was added dropwise to a mixture of H_2O and TPAOH under vigorous stirring, giving rise to a clear solution. Then, tetrabutylorthotitanate (TBOT) and ethanol were added dropwise to this solution. After the complete hydrolysis of TEOS and TBOT, a certain amount of active seeds or calcined seeds (2 wt%, based on SiO_2) was added into the mixture under vigorous stirring. Finally, the resulting solution was transferred into a Teflon vessel and crystallized at 170 °C in a microwave reactor for 1 h under static conditions. The sample synthesized *via* the combination of the active seeds assistance and microwave irradiation was denoted as TS-1-AM. The sample synthesized *via* the combination of the calcined seeds assistance and microwave irradiation was denoted as TS-1-CM.

Preparation of TS-1-A, TS-1-M

As for TS-1-A and TS-1-M, they were prepared with the same synthesis procedure as described above by solely using the active seeds assistance under conventional hydrothermal conditions (1 h) and microwave irradiation conditions (1 h), respectively.

Catalytic tests

The epoxidation of 1-hexene with H_2O_2 was carried out in a 25 mL two-necked round-bottom-flask equipped with a reflux condenser under vigorous stirring and at atmospheric pressure. In a typical run, 10 mL of methanol, 10 mmol of 1-hexene, 10 mmol of H_2O_2 (30 wt%), and 50 mg of the catalyst were mixed in the flask, and the reaction was run under magnetic stirring at 333 K. After the completion of the reaction, the liquid products were separated by centrifugation and analyzed with a gas chromatograph (Agilent 6890N), equipped with a 30 m capillary column (HP-5MS) and an FID detector using chlorobenzene as an internal standard. The conversion of 1-hexene and the selectivity of epoxides were calculated accordingly. All the products were confirmed by GC-MS (Thermo Fisher Trace ISQ).

In the recycling tests of the 1-hexene epoxidation reaction, the used catalyst was dried overnight at 353 K and calcined in air at 823 K for 6 h for the next use.

Results and discussion

By combining the active seeds assistance and microwave irradiation, highly catalytically active Ti species can be effectively created in well-crystallized TS-1 zeolite (denoted as TS-1-AM). In comparison, the conventional TS-1 (denoted as TS-1-C), the active seed-assisted conventional TS-1 (denoted as TS-1-A), and microwave-assisted TS-1 (denoted as TS-1-M) were prepared.

According to the powder X-ray diffraction (XRD) analysis, the conventional TS-1 zeolite normally requires 2–4 days for crystallization (Fig. S1†). In contrast, as shown in Fig. 1A, the TS-1 samples (TS-1-AM, TS-1-A, and TS-1-M) that crystallized in 1

hour show much stronger diffraction peaks of the **MFI** structure than TS-1-C (1.5 hours crystallization),[35] indicating that both active seeds and microwave irradiation can accelerate the crystallization of TS-1 zeolites. Noteworthily, TS-1-AM (1 h) exhibits almost the same peak intensity as that of the conventional TS-1-C (4 days), which indicates the high crystallinity of TS-1-AM assisted by the active seeds and microwave irradiation.

Fourier-transform infrared spectroscopy (FT-IR) was performed to characterize the formation of the **MFI** structure and understand the level of titanium incorporation in the framework. As shown in Fig. 1B, the typical bands at 550 and 800 cm^{-1} appear in all the TS-1 sample spectra, which are attributed to the stretching vibration of double rings and [SiO_4] units in the **MFI** structure.[36] Moreover, the characteristic band at 960 cm^{-1}, which is assigned to the vibration of Si–O–Ti or Si–O bond perturbed by Ti atoms in the framework, was observed in the FT-IR spectra.[37,38] To evaluate the relative contents of the framework titanium in different TS-1 zeolites, the intensity ratios of the absorption band at 960 cm^{-1} to that at 800 cm^{-1} ($I_{960/800}$) were obtained, are summarized in Table 1. In general, a higher incorporation degree of the framework Ti gives rise to a larger $I_{960/800}$. Compared with TS-1-C, TS-1-AM, and TS-1-A, TS-1-M shows a lower $I_{960/800}$ value (0.62), indicating that less Ti can be properly inserted into the framework of the TS-1 zeolite under the sole assistance of microwave irradiation.

According to the transmission electron microscopy (TEM) and scanning electron microscopy (SEM) images (Fig. 2 and S2†), TS-1-AM and TS-1-M possess a crystal size (ca. 150 nm) similar to that of TS-1-C. However, TS-1-A displays relatively smaller crystals with a quite rough surface.

The nitrogen adsorption–desorption isotherms of different TS-1 zeolites are shown in Fig. S3.† A clear hysteresis loop near the saturation pressure ($0.8 < P/P_0 < 0.99$) was observed for all the TS-1 samples, suggesting the existence of interparticle voids caused by the stacking of the nano-sized TS-1 crystals. According to the textural properties summarized in Table S1,† TS-1-A exhibits a smaller micropore surface area (234.9 $m^2\ g^{-1}$) and micropore volume (0.11 $cm^3\ g^{-1}$) than the well-crystallized TS-1 zeolites, including TS-1-C, TS-1-AM, and TS-1-M (270–280 $m^2\ g^{-1}$, 0.13 $cm^3\ g^{-1}$), revealing the incomplete crystallization of TS-1-A (1 h). This finding is in accordance with the TEM result.

To probe the chemical environments of the Ti species in different TS-1 zeolites, various spectroscopic techniques were employed. As shown in the ultraviolet-visible diffuse reflectance (UV-vis) spectra (Fig. 3A), two main absorption bands at around

Table 1 Epoxidation of 1-hexene over different TS-1 samples[d]

				Sel. (%)		
	$I_{960/800}$[a]	Si/Ti[b]	Conv. (%)	Epoxide	Others	TON[c]
TS-1-C	1.03	70	18.8	93.2	6.8	161
TS-1-AM	1.10	80	28.0	90.0	10.0	272
TS-1-A	0.98	87	12.3	94.7	5.3	131
TS-1-M	0.62	73	12.2	94.5	5.6	110

[a] $I_{960/800}$ is used to estimate the relative content of framework Ti. [b] The elemental compositions are determined by XRF. [c] TON in mol per mol of Ti, turnover number per Ti site for 1-hexene conversion. [d] Reactions conditions: catalyst 50 mg, 1-hexene 10 mmol, H_2O_2 10 mmol, CH_3OH 10 mL, temp. 333 K, time 2 h. Others, 1-methoxyhexan-2-ol, 2-methoxyhexan-1-ol, 1,2-hexanediol.

210 and 330 nm were observed for TS-1-C, indicating the existence of the tetrahedral-coordinated framework Ti species (TiO_4) and anatase TiO_2.[39–41] Interestingly, a new absorption band around 250–290 nm appeared in TS-1-A and TS-1-AM, which is commonly attributed to the formation of high (penta- or octahedral) – coordinated Ti species.[21] These results suggest that adding active seeds is beneficial for building high-coordinated Ti species. With regard to TS-1-M, the Ti species distribution is similar to that in TS-1-C, except the appearance of a more significant characteristic band of anatase TiO_2. Even though microwave assistance can greatly boost the crystallization rate of TS-1 zeolite, it will cause a severe mismatch between the formation rate of the **MFI** structure and insertion rate of Ti ions.[16] Consequently, more anatase TiO_2 will form during this process.

To get further insights on the high-coordinated Ti species, ultraviolet resonance Raman (UV-Raman) spectra of different

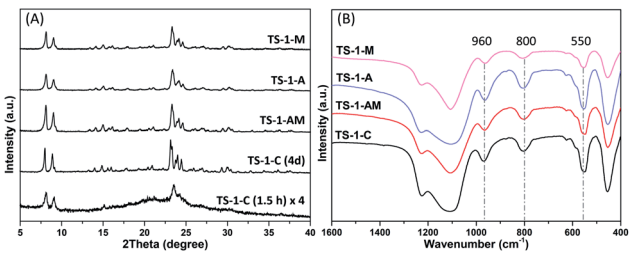

Fig. 1 The XRD patterns (A) and FT-IR spectra (B) of different TS-1 samples.

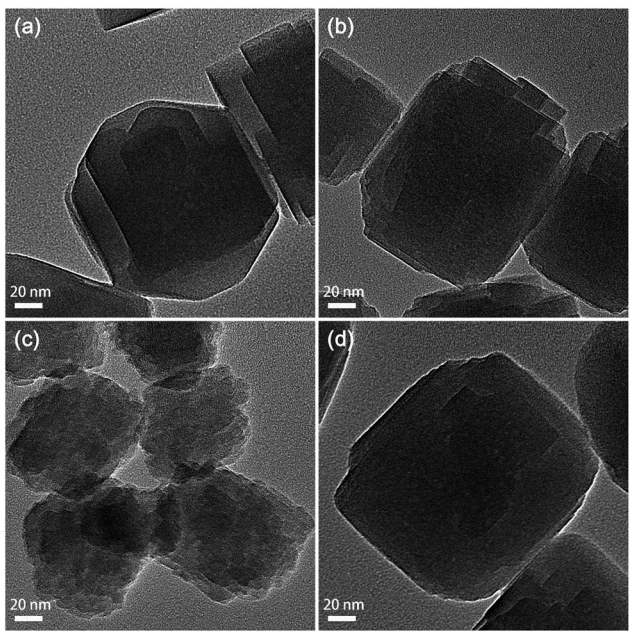

Fig. 2 The TEM images of TS-1-C (a), TS-1-AM (b), TS-1-A (c), and TS-1-M (d) zeolites.

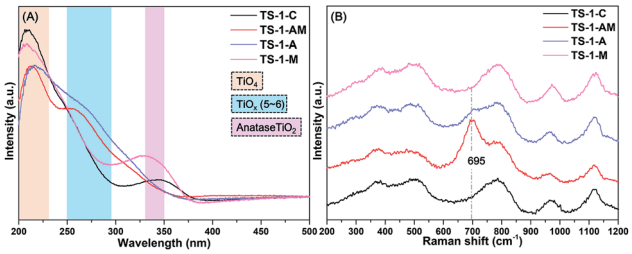

Fig. 3 UV-vis (A) and UV-Raman spectra (B) of TS-1-C, TS-1-AM, TS-1-A, and TS-1-M zeolites.

TS-1 zeolites were also collected (Fig. 3B). It is reported that the Raman band at 695 cm^{-1} was associated with the so-called "mononuclear TiO_6" based on the DFT calculations.[25,28] Such characteristic bands can be clearly found in TS-1-AM, notably, a weak shoulder band at 695 cm^{-1} was also observed in TS-1-A. These results suggest that adding active seeds can induce the formation of "mononuclear TiO_6" during the crystallization of TS-1 zeolites, and microwave irradiation can effectively boost the generation of TiO_6 in this process. Further analysis on the Ti species distributions in TS-1 zeolites, based on the X-ray photoelectron spectroscopy (XPS), was found to be in good agreement with the above results (Fig. S4†).

The coordination environment and local structure of the Ti species in TS-1 zeolites were further studied by collecting the XAS spectra at the Ti K edge. The X-ray absorption near edge structure (XANES) can probe the symmetry of the Ti coordination structure in a qualitative manner by the comparison of the pre-edge peaks (around 4960–4980 eV) with those of the reference materials,[31] including Ti foil, anatase TiO_2, and pure tetrahedral-coordinated TS-1 zeolite – TS-1-TiO_4 (Fig. S5†). In general, the more symmetrical structure of the Ti species leads to the more intense pre-edge peaks.[42,43] As shown in Fig. 4, the highest single peak can be observed in TS-1-TiO_4, which is due to the symmetrical structure of TiO_4.[44] In the case of anatase TiO_2, the pre-edge features give rise to three weak peaks denoted as A_1, A_2, and A_3.[45] As for TS-1-AM, compared with TS-1-TiO_4, the single pre-edge peak somewhat decreases, which should be attributed to the formation of a part of distorted species (TiO_6). With respect to TS-1-C, the intensity of such peak further decreases, which indicates the formation of a more distorted Ti species. Moreover, a weak peak appears at the same position of A_3 in anatase TiO_2, suggesting the presence of anatase TiO_2 in TS-1-C. In the post-edge region, TS-1-TiO_4 and TS-1-AM show much less distinct features than those of TS-1-C and anatase TiO_2. The lack of distinct features in this area can be explained by the loss of long- and medium-range ordered structures. That is to say, Ti is more dispersed in TS-1-TiO_4 and TS-1-AM.

As shown in Fig. 5, the Fourier-transformed extended X-ray absorption fine structure spectra (FT-EXAFS) of TS-1-AM show a major peak of the Ti–O bond, while no obvious Ti–Ti bonds were detected, in sharp contrast to TS-1-C. These results directly confirm that all Ti atoms were isolated in TS-1-AM, which is the most important feature of the titanium silicate catalysts. Moreover, the best fit of the obtained EXAFS data (Fig. S6 and Table S2†) reveals that the coordination number of Ti–O shell in TS-1-AM (4.3) was larger than that of TS-1-TiO_4 (4), which should be attributed to the formation of the high coordinated TiO_6 species in TS-1-AM along with the framework TiO_4 species.

The wavelet transform (WT)-EXAFS is a powerful method for separating backscattering atoms that provides not only a radial distance resolution but also the resolution in *k*-space.[31] As shown in Fig. 6, it can be observed that the WT maximum corresponding to the Ti–Ti shell was not observed for TS-1-AM in the interval from 2.5 to 3.7 Å, verifying the absence of Ti–Ti coordination. Therefore, the Ti atoms in TS-1 were homogeneously substituted into the T sites of the **MFI** framework without any occupation of adjacent T sites in pairs. As a consequence, the local structure of newly detected TiO_6 can be solidly confirmed as a kind of mononuclear Ti species.

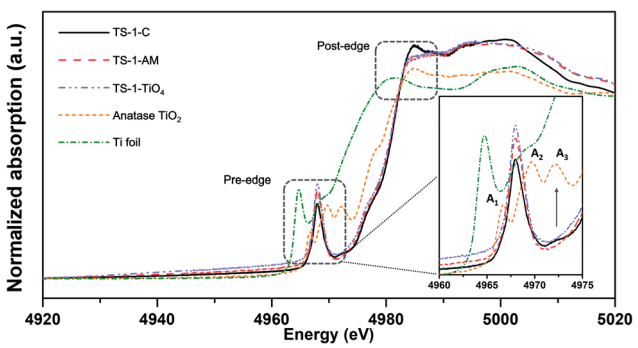

Fig. 4 Ti K-edge XANES spectra of different TS-1 samples, anatase TiO_2, and Ti foil reference.

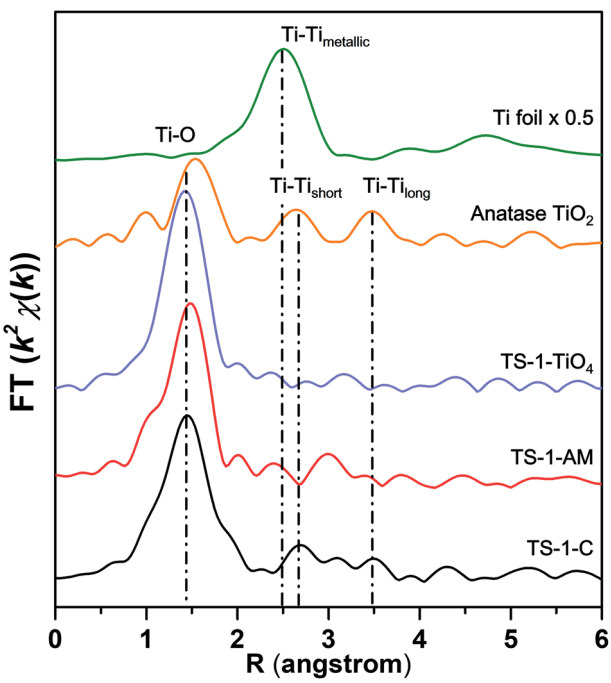

Fig. 5 Fourier transform k^2-weighted Ti EXAFS spectra in the R-spacing of different TS-1 samples, anatase TiO_2, and Ti foil reference.

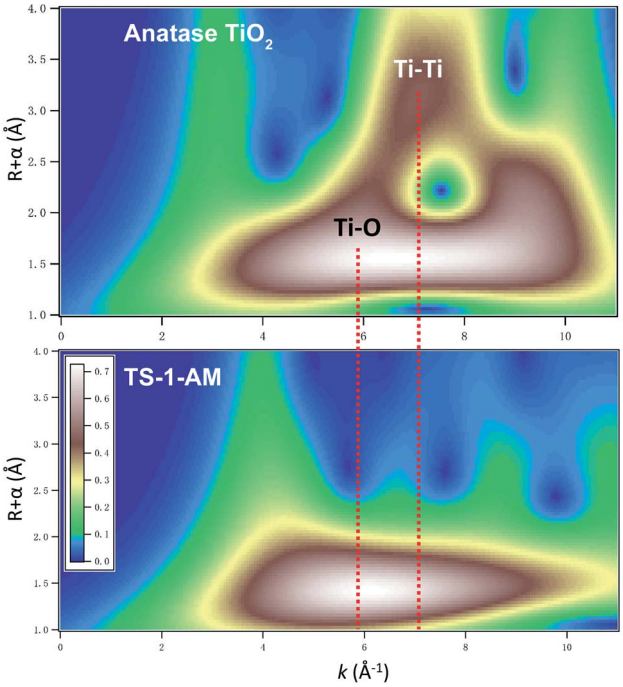

Fig. 6 Wavelet transform (WT) of TS-1-AM and anatase TiO_2. The WT contour plots are based on Morlet wavelets ($\kappa = 6$, $\sigma = 0.8$). The vertical dashed lines point out the k-space position of the Ti–O and Ti–Ti contributions.

The change of the coordination states of the Ti species in TS-1 zeolites, *i.e.*, before and after calcination, were addressed by the UV-vis spectra (Fig. 7). Interestingly, it seems that high coordinated Ti species exist in the TS-1-C, TS-1-AM, TS-1-A, and TS-1-M samples before calcination, evidenced by the absorption band around 250–290 nm. According to the literature, such kind of Ti species is weakly coordinated by organic template molecules or water ligands.[46,47] No evident peak around 330 nm can be found in the spectra of the samples before calcination, indicating the absence of anatase TiO_2 in the as-synthesized TS-1 zeolites. After calcination, however, significant broadband occurs around 330 nm in TS-1-C and TS-1-M. This might be due to the fact that the high coordinated Ti species in TS-1-C and TS-1-M were not stable and may condense and aggregate to form anatase TiO_2 upon calcination.[48] For TS-1-A, it can be observed that, after calcination, the spectrum becomes broader, indicating that a part of high coordinated Ti species was unstable. Notably, the UV-vis spectrum of TS-1-AM remains almost unchanged upon calcination. It can be inferred that the high coordinated Ti species, which has been characterized as mononuclear TiO_6, was highly stable.

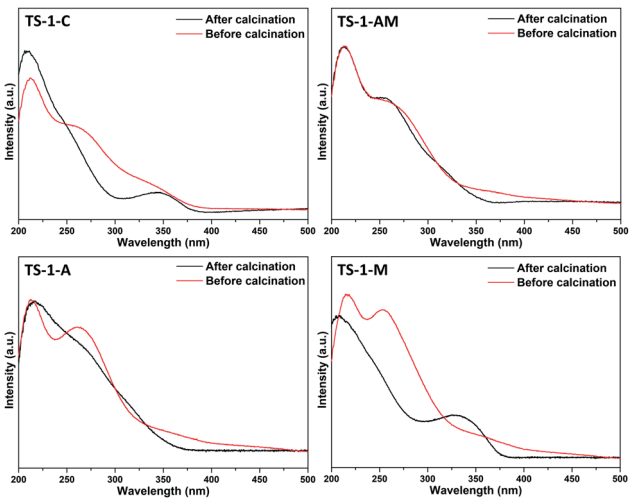

Fig. 7 UV-vis spectra of TS-1-C, TS-1-AM, TS-1-A, and TS-1-M zeolites before and after calcination.

Furthermore, the formation process of such unique mononuclear TiO_6 species was investigated in depth (Fig. 8). The XRD pattern of the active seeds barely shows the diffraction peaks of the **MFI** structure (Fig. 8A). However, the characteristic band (550 cm^{-1}) of double rings of the **MFI** structure appears in the FT-IR spectrum (Fig. 8B), suggesting that this colloidal state material was abundant in zeolitic fragments. An intense peak at 270 nm was detected in the UV-vis spectrum (Fig. 8C), demonstrating that plenty of high-coordinated Ti species exist in the active seeds. Such Ti species plays a crucial role in inducing the generation of mononuclear TiO_6 species. In addition, early literature reported that the Ti–O bond ($\Delta\chi = 2.18$) is a better microwave absorber than the Si–O bond ($\Delta\chi = 1.76$).[49] Thus, more high-coordinated Ti species can be strongly activated to form a stable mononuclear TiO_6 under microwave irradiation. In comparison, we replaced the active seeds with calcined seeds in such a synthesis system. The resultant product (TS-1-CM) possessed high crystallinity and main framework TiO_4 distribution (Fig. S7 and S8†). However, the high-coordinated Ti species was absent in such a catalyst. Compared with TS-1-AM, TS-1-CM exhibits lower catalytic activity in the 1-hexene epoxidation reaction (Table S3†). Therefore, the calcined seeds cannot take effect on the generation of highly active mononuclear TiO_6 species in TS-1.

The epoxidation of 1-hexene was further employed to evaluate the catalytic properties of different TS-1 zeolites (Table 1). The elemental analysis by X-ray fluorescence spectrometry (XRF) shows that TS-1-AM (Si/Ti = 80) possesses relatively lower Ti-content than TS-1-C (Si/Ti = 70). However, the 1-hexene conversion over TS-1-AM shows a significant increase than that over TS-1-C (TS-1-AM: 28.0% *vs.* TS-1-C: 18.8%) and the selectivity of epoxide product for these two catalysts stays at the same level. The turnover number (TON) values were calculated to further elucidate the intrinsic activity of the catalysts. TS-1-AM

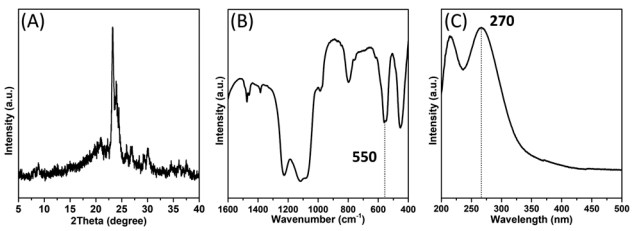

Fig. 8 The XRD pattern (A), FT-IR (B) and UV-vis (C) spectra of active seeds.

gives the TON of 1-hexene up to 272, which is almost 70% higher than that of TS-1-C (161). Furthermore, we found that the catalytic activity of TS-1-AM was also higher than that of TS-1-TiO_4, which only contains the framework TiO_4 (Fig. S5 and Table S4†). It is reported that the mononuclear TiO_6 species (open Ti sites) is more active than the framework TiO_4 species (close Ti sites) in alkene epoxidation reactions (Fig. 9).[25] As proved above, the main difference between TS-1-TiO_4 and TS-1-AM lies in the mononuclear TiO_6 species. Therefore, such novel active Ti centers should be responsible for the promoted catalytic activity. In contrast, the catalytic properties of TS-1-A and TS-1-M were suppressed, which should be explained by the incomplete crystallization and high content of anatase TiO_2, respectively. In addition, the catalytic performance of highly crystalline TS-1-A crystallized for 4 d was still poor due to the harmful anatase TiO_2 formed under the conventional crystallization condition (Fig. S9 and Table S4†).

The catalytic performance of TS-1-AM with various Ti contents was also investigated (Fig. S10†). With an increase in the Ti content, the 1-hexene conversion gradually improves. However, when the ratio of Ti/(Si + Ti) was higher than 0.0124, the TON slightly decreases. Due to the highly catalytic active mononuclear TiO_6 species, which is a kind of open Ti sites, the content of accessible mononuclear TiO_6 might be limited. Therefore, the optimized Ti content of TS-1-AM zeolites was Ti/(Si + Ti) = 0.0093–0.0124.

The stability of TS-1-AM was investigated in 1-hexene epoxidation. As shown in Fig. 10A, the 1-hexene conversion and 1, 2-epoxyhexane selectivity of TS-1-AM stays almost the same after 5 times of reuse. In addition, even after 5-time regeneration under the calcination condition, the UV-vis spectra (Fig. 10B) demonstrates that the highly active Ti species (λ = 260 nm) in the used catalyst stays stable, without the formation of anatase TiO_2. Furthermore, the XRD and FT-IR analyses indicate that TS-1-AM remains well-structured after the durability test (Fig. S11†).

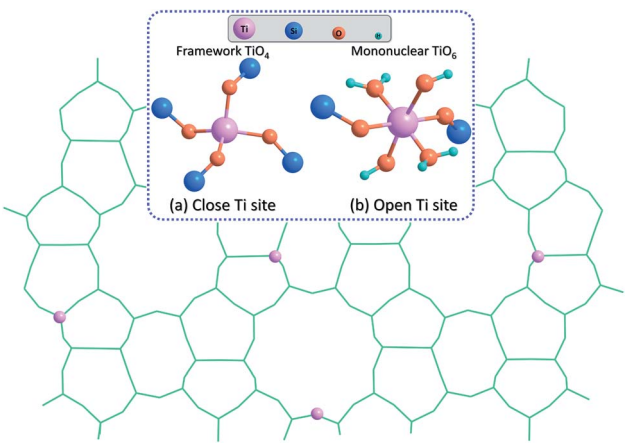

Fig. 9 Proposed titanium active sites in TS-1: (a) closed Ti site and (b) open Ti site.

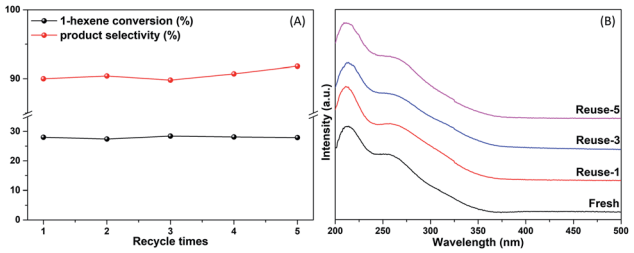

Fig. 10 The catalytic activity of 1-hexene epoxidation (A) and UV-vis spectra (B) of fresh and reused TS-1-AM.

Conclusions

In conclusion, the one-step rapid synthesis of the TS-1 zeolite with highly catalytic active Ti species was achieved by introducing active seeds and microwave irradiation. Based on the UV-vis and UV-Raman spectra, the novel octahedral-coordinated Ti species (TiO_6) was present in resultant TS-1 zeolites. The mononuclear state of TiO_6 species was further determined by X-ray absorption spectroscopy. The experimental studies reveal that adding active seeds can induce the formation of mononuclear TiO_6; on the other hand, the microwave irradiation will boost the generation of such TiO_6. The mononuclear TiO_6 species in the as-prepared TS-1 remain stable upon calcination, without the formation of anatase TiO_2. The TS-1 catalyst with mononuclear TiO_6 species exhibits outstanding catalytic activity and stability in 1-hexene epoxidation. This study offers a facile approach to modulate the coordination environment of Ti species in the Ti-containing zeolites, which will enlighten the rational synthesis and catalytic application of titanosilicate zeolites with highly catalytically active Ti sites.

Conflicts of interest

There are no conflicts to declare.

Acknowledgements

We thank the financial supports by the National Natural Science Foundation of China (Grant 21920102005, 21835002 and 21621001), the National Key Research and Development Program of China (Grant 2016YFB0701100), the 111 Project of (B17020). The APS was operated for the U.S. DOE Office of Science by Argonne National Laboratory, and the CLS@APS facilities (Sector 20) were supported by the U.S. DOE under Contract No. DEAC02-06CH11357, and the Canadian Light Source and its funding partners. Tianjun Zhang acknowledges the China Scholarship Council (CSC).

Notes and references

1 A. Corma, F. Rey, J. Rius, M. J. Sabater and S. Valencia, *Nature*, 2004, **431**, 287–290.
2 Z. Wang, J. H. Yu and R. R. Xu, *Chem. Soc. Rev.*, 2012, **41**, 1729–1741.

3 R. R. Xu, W. Q. Pang, J. H. Yu, Q. S. Huo and J. S. Chen, *Chemistry of zeolites and related porous materials*, John Wiley & Sons, (Asia) Pte Ltd, 2007.
4 M. G. Clerici, G. Bellussi and U. Romano, *J. Catal.*, 1991, **129**, 159–167.
5 Y. Kuwahara, K. Nishizawa, T. Nakajima, T. Kamegawa, K. Mori and H. Yamashita, *J. Am. Chem. Soc.*, 2011, **133**, 12462–12465.
6 L. Z. Wu, S. F. Zhao, L. F. Lin, X. P. Fang, Y. M. Liu and M. Y. He, *J. Catal.*, 2016, **337**, 248–259.
7 J. Kim, J. Chun and R. Ryoo, *Chem. Commun.*, 2015, **51**, 13102–13105.
8 N. Tsunoji, M. Opanasenko, M. Kubu, J. Čejka, H. Nishida, S. Hayakawa, Y. Ide, M. Sadakane and T. Sano, *ChemCatChem*, 2018, **10**, 2536–2540.
9 M. A. Mantegazza, G. Leofanti, G. Petrini, M. Padovan, A. Zecchina and S. Bordiga, *Stud. Surf. Sci. Catal.*, 1994, **82**, 541–550.
10 S. Inagaki, Y. Tsuboi, M. Sasaki, K. Mamiya, S. Park and Y. Kubota, *Green Chem.*, 2016, **18**, 735–741.
11 Y. Zuo, M. Liu, T. Zhang, C. G. Meng, X. W. Guo and C. S. Song, *ChemCatChem*, 2015, **7**, 2660–2668.
12 P. Wu, T. Tatsumi, T. Komatsu and T. Yashima, *J. Phys. Chem. B*, 2001, **105**, 2897–2905.
13 J. H. Ding and P. Wu, *Appl. Catal., A*, 2014, **488**, 86–95.
14 B. Tang, W. L. Dai, X. M. Sun, N. J. Guan, L. D. Li and M. Hunger, *Green Chem.*, 2014, **16**, 2281–2291.
15 J. Přech, *Catal. Rev.*, 2018, **60**, 71–131.
16 T. J. Zhang, X. X. Chen, G. R Chen, M. Y. Chen, R. S. Bai, M. J. Jia and J. H. Yu, *J. Mater. Chem. A*, 2018, **6**, 9473–9479.
17 D. H. Wells, W. N. Delgass and K. T. Thomson, *J. Am. Chem. Soc.*, 2004, **126**, 2956–2962.
18 Y. Zuo, W. C. Song, C. Y. Dai, Y. P. He, M. L. Wang, X. S. Wang and X. W. Guo, *Appl. Catal., A*, 2013, **453**, 272–279.
19 A. Korzeniowska, J. Grzybek, W. Roth, A. Kowalczyk, P. Michorczyk, J. Čejka, J. Přech and B. Gil, *ChemCatChem*, 2018, **10**, 1–9.
20 X. Q. Fang, Q. Wang, A. M. Zheng, Y. M. Liu, Y. N. Wang, X. J. Deng, H. H. Wu, F. Deng, M. Y. He and P. Wu, *Catal. Sci. Technol.*, 2012, **2**, 2433–2435.
21 M. Sasaki, Y. Sato, Y. Tsuboi, S. Inagaki and Y. Kubota, *ACS Catal.*, 2014, **4**, 2653–2657.
22 K. Y. Leng, Y. Y. Sun, X. Zhang, M. Yu and W. Xu, *Fuel*, 2016, **174**, 9–16.
23 X. Q. Fang, Q. Wang, A. M. Zheng, Y. M. Liu, L. F. Lin, H. H. Wu, F. Deng, M. Y. He and P. Wu, *Phys. Chem. Chem. Phys.*, 2013, **15**, 4930–4938.
24 Y. Wei, G. Li, R. M. Su, H. Lu and H. C. Guo, *Appl. Catal., A*, 2019, **582**, 117108.
25 L. Z. Wu, X. J. Deng, S. F. Zhao, H. M. Yin, Z. X. Zhuo, X. Q. Fang, Y. M. Liu and M. Y. He, *Chem. Commun.*, 2016, **52**, 8679–8682.
26 L. Xu, D. D. Huang, C. G. Li, X. Y. Ji, S. Q. Jin, Z. C. Feng, F. Xia, X. H. Li, F. T. Fan, C. Li and P. Wu, *Chem. Commun.*, 2015, **51**, 9010–9013.
27 Y. Zuo, M. Liu, T. Zhang, L. W. Hong, X. W. Guo, C. S. Song, Y. S. Chen, P. Y. Zhu, C. Jayec and D. Fischer, *RSC Adv.*, 2015, **5**, 17897–17904.
28 Q. Guo, K. J. Sun, Z. C. Feng, G. N. Li, M. L. Guo, F. T. Fan and C. Li, *Chem.–Eur. J.*, 2012, **18**, 13854–13860.
29 W. O. Parker and R. Millini, *J. Am. Chem. Soc.*, 2006, **128**, 1450–1451.
30 M. Signorile, V. Crocellà, A. Damin, B. Rossi, C. Lamberti, F. Bonino and S. Bordiga, *J. Phys. Chem. C*, 2018, **122**, 9021–9034.
31 J. Dong, H. L. Zhu, Y. J. Xiang, Y. Wang, P. F. An, Y. Gong, Y. X. Liang, L. M. Qiu, A. G. Zheng, X. X. Peng, M. Lin, G. T. Xu, Z. Y. Guo and D. L. Chen, *J. Phys. Chem. C*, 2016, **120**, 20114–20124.
32 A. C. Alba-Rubio, J. L. G. Fierro, L. León-Reina, R. Mariscal, J. A. Dumesic and M. L. Granados, *Appl. Catal., B*, 2017, **202**, 269–280.
33 Y. K. Hwang, J. S. Chang, S. E. Park, D. S. Kim, Y. U. Kwon, S. H. Jhung, J. S. Hwang and M. S. Park, *Angew. Chem., Int. Ed.*, 2005, **44**, 556–560.
34 R. S. Bai, Q. M. Sun, Y. Song, N. Wang, T. J. Zhang, F. Wang, Y. C. Zou, Z. C. Feng, S. Miao and J. H. Yu, *J. Mater. Chem. A*, 2018, **6**, 8757–8762.
35 S. T. Du, F. Li, Q. M. Sun, N. Wang, M. J. Jia and J. H. Yu, *Chem. Commun.*, 2016, **52**, 3368–3371.
36 X. Gao, J. G. An, J. L. Gu, L. Li and Y. S. Li, *Microporous Mesoporous Mater.*, 2017, **239**, 381–389.
37 P. Ratnasamy, D. Srinivas and H. Knozinger, *Adv. Catal.*, 2004, **48**, 1–169.
38 M. Liu, Z. H. Chang, H. J. Wei, B. J. Li, X. Y. Wang and Y. Q. Wen, *Appl. Catal., A*, 2016, **525**, 59–67.
39 C. Liu, J. L. Huang, D. H. Sun, Y. Zhou, X. L. Jing, M. M. Du, H. T. Wang and Q. B. Li, *Appl. Catal., A*, 2013, **459**, 1–7.
40 N. Tsunoji, H. Nishida, Y. Ide, K. Komaguchi, S. Hayakawa, Y. Yagenji, M. Sadakane and T. Sano, *ACS Catal.*, 2019, **9**, 5742–5751.
41 J. Přech, D. Vitvarová, L. Lupínková, M. Kubů and J. Čejka, *Microporous Mesoporous Mater.*, 2015, **212**, 28–34.
42 S. Bordiga, S. Coluccia, C. Lamberti, L. Marchese, A. Zecchina, F. Boscherini, F. Buffa, F. Genoni, G. Leofanti, G. Petrini and G. Vlaic, *J. Phys. Chem.*, 1994, **98**, 4125–4132.
43 S. Bordiga, F. Boscherini, S. Coluccia, F. Genoni, C. Lamberti, G. Leofanti, L. Marchese, G. Petrini, G. Vlaic and A. Zecchina, *Catal. Lett.*, 1994, **26**, 195–208.
44 H. K. D. Nguyen, G. Sankar and R. A. Catlow, *J. Porous Mater.*, 2017, **24**, 421–428.
45 F. Jin, C. C. Chang, C. W. Yang, J. F. Lee, L. Y. Jang and S. F. Cheng, *J. Mater. Chem. A*, 2015, **3**, 8715–8724.
46 F. Geobaldo, S. Bordiga, A. Zecchina, E. Giamello, G. Leofanti and G. Petrini, *Catal. Lett.*, 1992, **16**, 109–115.
47 L. Xu, D. D. Huang, C. G. Li, X. Y. Ji, S. Q. Jin, Z. C. Feng, F. Xia, X. H. Li, F. T. Fan, C. Li and P. Wu, *Chem. Commun.*, 2015, **51**, 9010–9013.
48 P. Wu, T. Tatsumi, T. Komatsu and T. Yashima, *J. Phys. Chem. C*, 2001, **105**, 2897–2905.
49 Z. Sun, T. Li, G. Li, Y. H. Zhang and Y. Tang, *RSC Adv.*, 2017, **7**, 35252–35256.